



Accepted Article

Title: Interfacially Bridging Covalent Network Yields Hyperstable and Ultralong Virus-based Fibers for Engineering Functional Materials

Authors: Qiangbin Wang, Kun Zhou, Yihao Zhou, Hongchao Yang, Huile Jin, and Yonggang Ke

This manuscript has been accepted after peer review and appears as an Accepted Article online prior to editing, proofing, and formal publication of the final Version of Record (VoR). This work is currently citable by using the Digital Object Identifier (DOI) given below. The VoR will be published online in Early View as soon as possible and may be different to this Accepted Article as a result of editing. Readers should obtain the VoR from the journal website shown below when it is published to ensure accuracy of information. The authors are responsible for the content of this Accepted Article.

To be cited as: Angew. Chem. Int. Ed. 10.1002/anie.202008670

Link to VoR: https://doi.org/10.1002/anie.202008670

Interfacially Bridging Covalent Network Yields Hyperstable and Ultralong Virus-based Fibers for Engineering Functional Materials

Kun Zhou^{†‡¶}, Yihao Zhou[‡]∥¶, Hongchao Yang[‡], Huile Jin^{†*}, Yonggang Ke^{§*}, and Qiangbin Wang[‡]∥*

†Institute of New Materials and Industrial Technologies, Wenzhou University, Wenzhou 325035,

China

‡CAS Key Laboratory of Nano-Bio Interface, Division of Nanobiomedicine and *i*-Lab, Suzhou Institute of Nano-Tech and Nano-Bionics, Chinese Academy of Sciences, Suzhou 215123, China §Wallace H. Coulter Department of Biomedical Engineering, Georgia Institute of Technology and Emory University, Atlanta, Georgia 30322, United States

"School of Nano-Tech and Nano-Bionics, University of Science and Technology of China, Hefei 230026, China

ABSTRACT: Virus and virus-like particles (VLPs) are very attractive biological subjects for self-assembly manipulation and templated synthesis of nanomaterials. However, the fundamental studies and applications are often constrained by problems associated with their structural weakness. Here we present a strategy of interfacially bridging covalent network within tobacco mosaic virus (TMV) VLPs to bring outstanding structural properties and functionalities. We arranged T103C cysteine to laterally conjugate adjacent subunits. In the axis direction, we set A74C mutation and systematically investigated candidate from E50C to P54C as the other thiol function site, for forming longitudinal disulfide bond chains. Significantly, the T103C-TMV-E50C-A74C shows the highest robustness in assembly capability and structural stability with the largest length, for TMV VLP to date. The fibers with lengths from several to a dozen of micrometers even survive under pH 13. The robust nature of this TMV VLP allows for reducer-free synthesis of excellent electrocatalysts for application in harshly alkaline hydrogen evolution. This study, therefore, presents significant progress to develop existing VLP with

unprecedented structural properties and the applications thereof.

KEYWORDS: tobacco mosaic virus; virus-like particle; covalent network; disulfide bond; structural stability

Virus and virus-like particle (VLP) have played prominent roles in nanotechnology research, particularly in the hierarchical assembly of highly organized scaffolds and template-directed synthesis. Despite much progress on these studies, a fundamentally important limitation in the development of virus-based nanomaterials is their physical metastability. Virus has naturally evolved an optimum compromise between stability and instability, which enables genome/capsid association and dissociation responsive to dynamic circumstances during its life cycles. While this trait hinders the application of VLPs when encountering relatively harsh conditions during production, storage or use.

Taking tobacco mosaic virus (TMV) – one of the most widely studied viral templates as an example, it has a 300 nm long tube structure with 18 nm outer and 4 nm inner diameters, capable of being a universal one-dimensional (1D) platform for synthesis and decoration of functional elements. ¹⁰⁻¹⁶ TMV has an uncoating mechanism: the electrostatic repulsion between the so-called "Caspar" carboxylate pairs act as a metastable switch for the stripping of TMV capsid upon entry into the cytosol. ^{17,18} Thus it is inherently sensitive toward alkali. ^{19,20} Strategies to reduce repulsive carboxyl-carboxylate inter-subunit interactions, e.g. E50Q/D77N mutations, have proven to mitigate the structural weakness, resulting in TMV VLP rods with lengths of several hundred nanometers stable at around pH 10. ^{18,21} Even though TMV VLP has shown potential for wide applications in biomedicine, ²²⁻²⁶ energy, ²⁷⁻³² and materials science, ³³⁻⁴² etc, it is apparently imperative to develop strategies for engineering hyperstable and ultralong TMV VLPs to extend their functionalities.

Here, we aim to precisely engineer covalent conjugation of TMV inter-subunit surfaces in both lateral and axial directions, in pursuit of covalent network for chaining all subunits into ultralong TMV rods, *i.e.* hyperstable TMV fibers (Figure 1). We laterally formed covalent

crosslinking between every two adjacent subunits by merely introducing a cysteine at the 103rd site (T103C) (Figure 1A).⁴³ In the axial direction, we chose the A74 position as a cysteine mutation site for introducing the thiol functionality (A74C), and then screened out the second candidate for cysteine mutation on the opposite surface ranging from E50 to P54 for longitudinal disulfide bond formation (Figure 1B, C). The obtained recombinant TMV proteins all form micrometer-sized fiber structures. The structures were systematically investigated by transmission electron microscope (TEM), non-reducing SDS-PAGE, circular dichroism, and alkaline treatment. Significantly, the T103C-TMV-E50C-A74C showed dramatically enhanced assembly capability and structure stability with above 12-µm fibers survived in pH 13 buffer. We further applied T103C-TMV-E50C-A74C fibers as templates for the reducing agent-free synthesis of Pd, Pt, and Pd-Pt electrocatalysts with tailorable ratios. The as-prepared Pd-Pt/TMV presented excellent electrochemical catalytic performance in alkaline hydrogen evolution reaction (HER) - an important half-cell reaction of electrochemical water splitting for hydrogen generation. To the best of our knowledge, this is the most robust TMV VLP structure, suggesting the success of our strategy of interfacially bridging the neighboring TMV subunits into the covalent network. Looking forward, we expect more applications of functional nanomaterials derived from this advanced TMV VLP.

RESULTS AND DISCUSSION

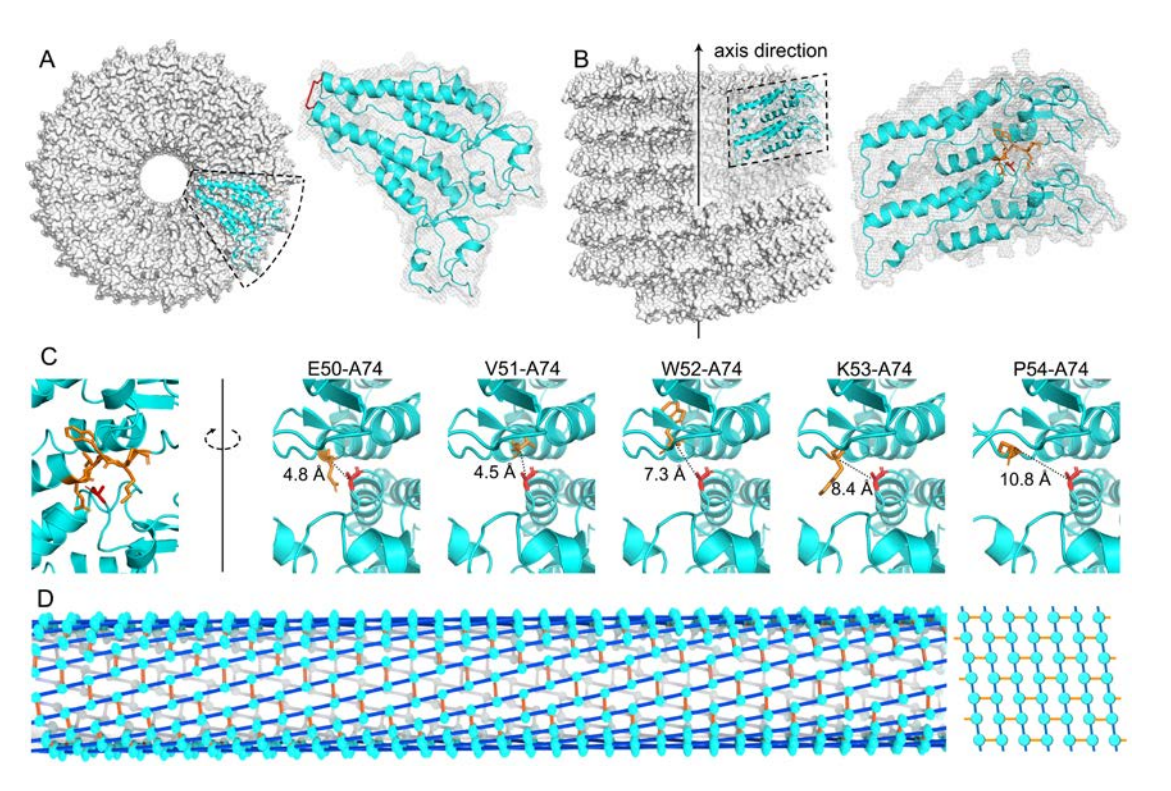


Figure 1. Design of interfacially bridging covalent network within TMV structure. (A) Top view of partial TMV protein assemblies and the molecular model of two neighboring T103C subunits that can covalently form a dimer by a disulfide bond (red) in the lateral direction. (B) Side view of partial TMV protein assemblies and the molecular model of two neighboring native TMV subunits, displaying the close proximity between target residues within $50\sim54$ (orange) and A74 (red) for engineering disulfide bonds along the axis direction. (C) Comparison of the interfacial interaction between the residues 50-54 (orange) and 74 (red), presenting the $C_{\alpha} - C_{\alpha}$ distances between residue pairs of E50-A74, V51-A74, W52-A74, K53-A74, and P54-A74. PDB code: 2OM3. (D) Simplified schematic diagram of partial covalent network crosslinking TMV subunits. The right figure indicates the plane surface. The TMV subunits are represented by cyan ellipsoids (left) and dots (right). The disulfide bonds in lateral and longitudinal directions are denoted with orange and dark blue sticks, respectively. Note that every two adjacent T103C Cys laterally form disulfide bonds that should present random uniform distribution within the covalent network.

We started the design by the analysis of TMV atomic models (PDB codes: 20M3, 3J06, 2TMV, 1EI7). The main difference between these structures occurs in the loop region and RNA binding zone at the lower radius, while the residues in the median radius zone are highly coincident (Figure S1A). We examined the most compact region of the longitudinal interfaces at the median

radius, in the hope of engineering and making the interfaces covalently interlocked but non-overlapping. We chose A74 for cysteine (Cys) mutagenesis because of its most protruding location and correct orientation of the side chain out toward the subunit on the other side in the axis direction, which could provide minimal structural perturbation. In addition, the Ala is most analogous to Cys in the region from 72nd to 76th sites (residues: YNAVL), which means negligible impact on the alteration regarding hydrophobic and electrostatic interactions. As for the longitudinally neighboring Cys candidate, we targeted the residue region from E50 to P54, in which the residue comes out from the end of an α -helix to a loop zone and has potential to overcome the distance and steric constraint. As shown in Figure 1C, this part is in close proximity to A74 and thus favorable for forming Cys – Cys disulfide bonds (C_{α} – C_{α} distances <11 Å). In combination with T103C Cys for the lateral disulfide bond design, ⁴³ we engineered five variants: T103C-TMV-E50C-A74C, T103C-TMV-V51C-A74C, T103C-TMV-W52C-A74C, T103C-TMV-K53C-A74C, and T103C-TMV-P54C-A74C, in which T103C-TMV-W52C-A74C was expressed totally as inclusion body very likely due to the alteration of the buried hydrophobic residue cluster (Figure S2).

Self-assembly of T103C-TMV-E50C-A74C, T103C-TMV-V51C-A74C. T103C-TMV-K53C-A74C, and T103C-TMV-P54C-A74C were conducted in 50 mM phosphate buffer (PB) with pH 5.5 known to produce short nanorods for WT-TMV. Divalent copper ion was used to promote the oxidation of sulfhydryl groups. 44 All four mutants generated fibrous structures with length of several micrometers in one day while differing in assembly efficiency and quality (Figure 2 and Figure S3-S5). T103C-TMV-E50C-A74C all assembled into rigid defectless fibers. T103C-TMV-V51C-A74C presented rigid fibers, along with free disks and aggregates thereof. T103C-TMV-K53C-A74C all assembled into fibers but with a lot of nicks. T103C-TMV-P54C-A74C formed disk aggregates and cracked fibers. Without the use of the oxidation promoter (CuCl₂), longer incubation time (e.g., three weeks) was required for the formation of fiber structures (Figure S6), except for T103C-TMV-E50C-A74C that formed fibers in one day even at pH 7 (Figure S7). Clearly, the T103C-TMV-E50C-A74C has exhibited remarkable assembly property.

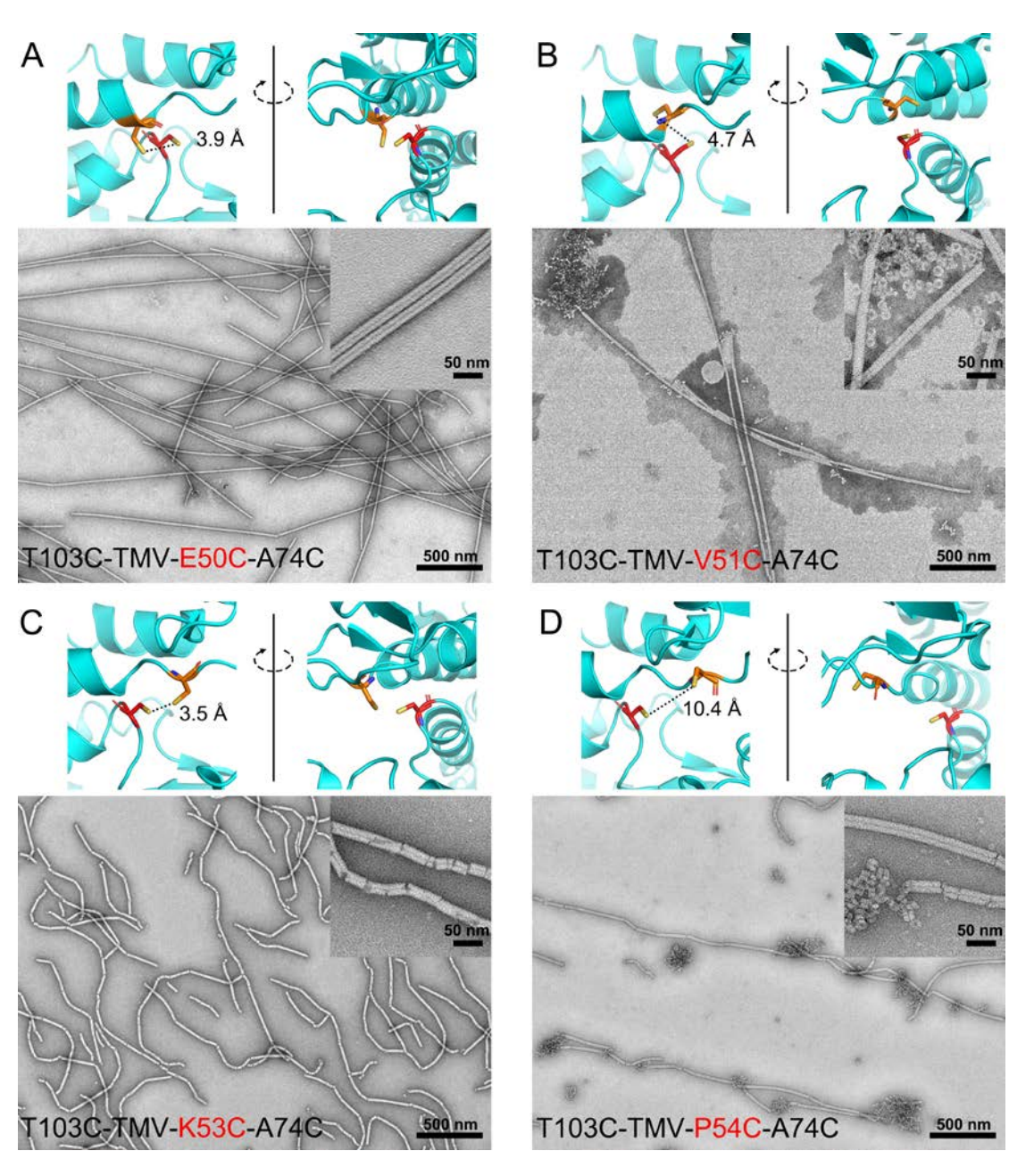


Figure 2. Comparison of four variants of T103C-TMV-E50C-A74C (A), T103C-TMV-V51C-A74C (B), T103C-TMV-K53C-A74C (C), and T103C-TMV-P54C-A74C (D). Upper panels: the close-up views of structure molecular models generated using PyMOL mutagenesis. The distances between the sulfur atoms of C50-C74, C51-C74, C53-C74, and C54-C74 pairs are labeled in the figures. Lower panels: the typical TEM images showing the assembly status of proteins in pH 5.5, 50 mM PB supplemented with 50 μM CuCl₂.

Distance between the neighboring Cys sulfur atoms strongly predicts disulfide bond formation. When two thiols are \leq 6.2 Å apart, there is a high probability that the Cys will become oxidized

into disulfide. 45 We measured the distance between the thiol groups using PyMOL. 46 The S – S distances of C50-C74 and C53-C74 are both less than 4 Å (Figure 2A and 2C, upper panels), which are short enough for disulfide bond formation, resulting in their high assembly efficiency of fiber conformation. The C50 and C74 stand closely side by side and face the same direction (Figure 2A), and therefore can overcome minimal structural constraint for forming a disulfide bond of 2.05 Å distance. However, the linkage of C53 to C74 should stretch multiple residues next to C53 (Figure 2C). In this case, it requires more interface coordination work between disks which presumably gave rise to the numerous nicks in T103C-TMV-K53C-A74C fiber structure. The S – S distances of C51-C74 and C54-C74 are 4.7 Å and 10.4 Å, respectively. The longer distance apparently makes them hardly form disulfide bond. Besides the distance, the degree of solvent exposure infers oxidation susceptibility of the thiols. 45,47 We calculated the relative solvent accessibility (RSA) for all residues (Table S1). There is one native Cys at the 27th site (C27) in TMV structure which is highly buried and has only 2% RSA, consistent with its very poor reactivity in the previous study.⁴⁸ The RSA values of C50, C51, C53, and C54 are 81%, 21%, 54%, and 31%, respectively, in association with 81% RSA for C74 and 67% RSA for C103 in the designed structures (Table S1). Larger accessible surface areas of C50, C53, and C74 make them sensitive to further oxidation. It stands to the results that T103C-TMV-E50C-A74C and T103C-TMV-K53C-A74C have better assembly ability.

We further examined these disulfide bonds formed at neighboring interfaces of TMV subunits using non-reducing SDS-PAGE. As shown in Figure 3A, samples dealt with DTT in the loading buffer led to one band referring to the monomer state. Whereas under non-reducing conditions, the bands with slower mobility shifts indicate the covalent polymerization of subunits via disulfide bonds. As expected, T103C-TMV gave a main dimer band which proved the formation of C103-C103 disulfide bond in the lateral direction. The T103C-TMV-E50C-A74C caused large aggregates almost completely stuck even in the stacking gel well, confirming severe polymerization of subunits by numerous disulfide bonds. For T103C-TMV-V51C-A74C, T103C-TMV-K53C-A74C, and T103C-TMV-P54C-A74C, they showed multiple bands as well as the bands stuck in the gel wells in contrast to the T103C-TMV, indicating the disulfide bond-induced protein oligopolymers. Nevertheless, some protein oligopolymers in T103C-TMV-V51C-A74C and T103C-TMV-P54C-A74C may originate from their incorrect disk

aggregates by copper ion-inducted fast oxidation as shown in Figure 2B and 2D. We thus performed non-reducing SDS-PAGE for the samples assembled in the absence of copper ion but with a longer incubation period of three weeks (Figure 3A, rightmost four lanes). T103C-TMV-V50C-A74C and T103C-TMV-K53C-A74C have gel results very similar to the previous Cu²⁺-catalyzed ones. While, for T103C-TMV-V51C-A74C and T103C-TMV-P54C-A74C, there was barely any band stuck in the gel wells and the decrease in band intensities of polymerized proteins was observed, especially for T103C-TMV-P54C-A74C. This agrees with their lower efficiency for disulfide bond formation and fiber assembly, compared with T103C-TMV-V50C-A74C and T103C-TMV-K53C-A74C.

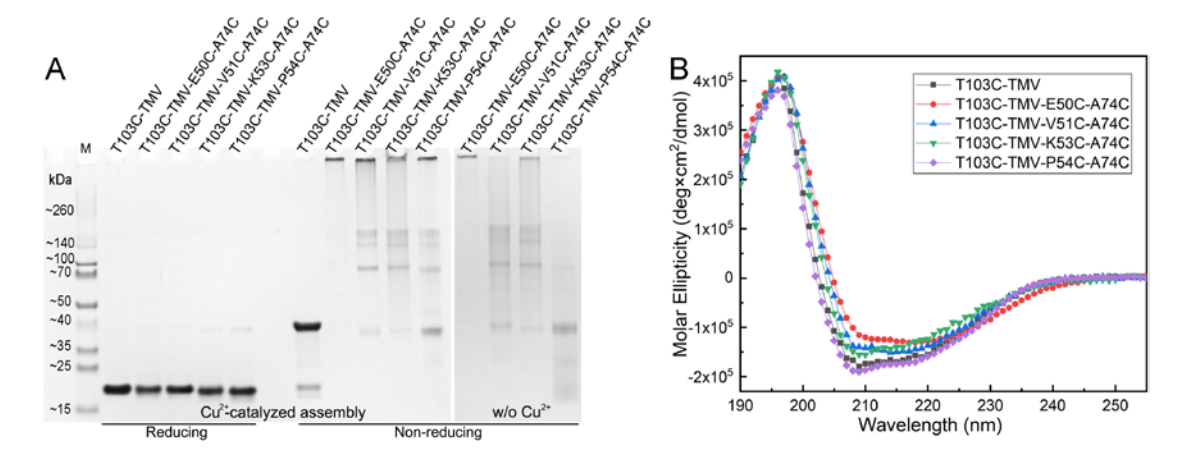


Figure 3. (A) Non-reducing SDS-PAGE analysis for the assessment of disulfide bond network. Cu²⁺-catalyzed assembly samples are assembled in pH 5.5, 50 mM PB with 50 μM CuCl₂ for one day. The rightmost four samples are assembled in pH 5.5, 50 mM PB for three weeks. For reducing SDS-PAGE, the loading buffer with DTT was used while no DTT was used in the loading buffer for non-reducing SDS-PAGE. (B) Far UV CD spectra of TMV variants, assembled in pH 5.5, 50 mM PB for three weeks.

Circular dichroism (CD) spectroscopy was used to examine the structures. As shown in Figure 3B, the T103C-TMV has a result similar to typical TMV protein rod or disk which have been reported in the previous works. $^{49-51}$ The CD spectrum shows a negative band at 208 nm and a shoulder near 222 nm, which are typical for protein with a high content of α -helices. The CD spectra of T103C-TMV and T103C-TMV-P54C-A74C overlay identically, suggesting in general there is no secondary structure deviation between them. The CD spectra show slight differences

for T103C-TMV-E50C-A74C, T103C-TMV-V51C-A74C, and T103C-TMV-K53C-A74C, in comparison with T103C-TMV. The shift of the negative maximum from 208 to about 218 and 214 nm are observed for T103C-TMV-E50C-A74C and T103C-TMV-V51C-A74C, respectively. Such changes are usually found in proteins with the conversion of increase in β-structure content. For TMV structure, it may arise from more tight stacking of subunits.⁵² The negative maximum of T103C-TMV-K53C-A74C CD data is still at 208 nm but decreases slightly about 18000 deg·cm²·dmol⁻¹ and the signal at 222 nm drops about 31000 deg·cm²·dmol⁻¹. We speculate that the formation of C53-C74 disulfide bond could make the local residue region more stable and somewhat affects the α-helix zone originally ending at the 50th site.

T103C-TMV-E50C-A74C has shown the best assembly potential in these four designed variants. This greatly encourages us to test its self-assembly behavior at higher pH values. As shown in Figure 4A and Figure S8, T103C-TMV-E50C-A74C did assemble into long fibers under alkaline conditions with pH up to 9. The formation of disulfide bond network within the T103C-TMV-E50C-A74C subunits was confirmed by non-reducing SDS-PAGE results (Figure S9). These results further confirmed that T103C-TMV-E50C-A74C has dramatically improved assembly capability.

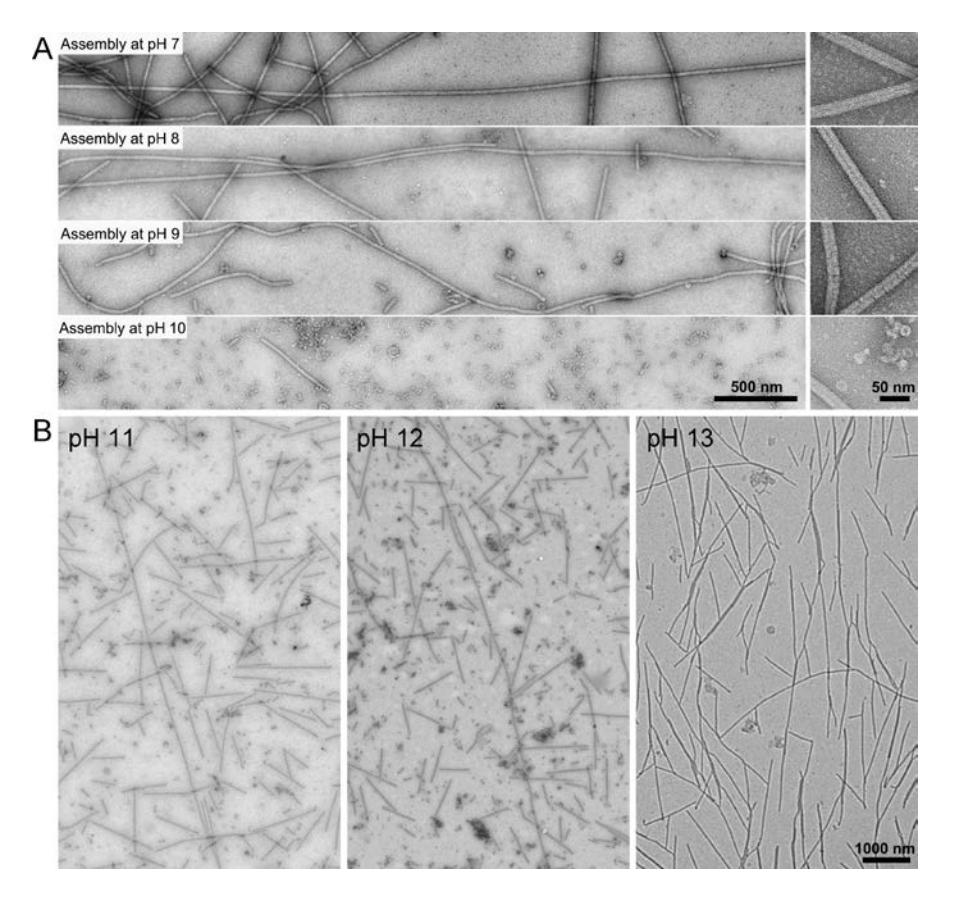


Figure 4. Characterization of T103C-TMV-E50C-A74C with significantly improved assembly efficiency and alkali resistance. (A) Assembly of T103C-TMV-E50C-A74C at pH 7, 8, 9, and 10 buffers, respectively. (B) Alkaline stability test of T103C-TMV-E50C-A74C fibers at pH 11 (left), pH 12 (middle), and pH 13 (right).

According to our design, ideally, the C50-C74 disulfide bonds will longitudinally chain all of the subunits. To characterize the covalent conjugations bridging axial interfaces, we got fiber precipitate by centrifugation (20000 g, 30 min) and quickly pipetted it hundred times to cause possible physical damage. Interestingly, the ultrafine protein fibers clearly appeared at the broken zones, however, maintained the fiber structures (Figure S10). It strongly indicates the covalent coupling of inter-subunits in the axis direction. Further, we investigated the stability of T103C-TMV-E50C-A74C fibers against alkali, as shown in Figure 4B. The structures with length of a dozen of micrometers even survived under the pH 13 condition (Figure S11).

E50Q/D77N mutations have proven to reduce the electrostatic repulsion between TMV subunits.²¹ Thus one may be curious about the similar effect on T103C-TMV-E50C-A74C that contributes to its enhanced inter-subunit association. We constructed T103C-TMV-E50Q,

T103C-TMV-E50Q-D77N and T103C-TMV-A74C (Figure S12). Unfortunately, we did not observe significantly elongated structure for both T103C-TMV-E50Q and T103C-TMV-E50Q-D77N compared to T103C-TMV. There were sporadic rods with lengths of several hundred nanometers in the T103C-TMV-E50Q-D77N sample, but still a lot of short rods and disks existed. In the absence of the C50 for paring C74, T103C-TMV-A74C formed short rods and disks. These results reflect the critical roles of Cys at 50th and 74th sites and the resultant disulfide bond in assembling T103C-TMV-E50C-A74C long fibers and the stabilizing effect. Indeed, the dithiothreitol (DTT) treatment disassemble the fibers by disulfide bond reduction (Figure S13).

Taking advantage of its high aspect ratio and outstanding stability, we further applied T103C-TMV-E50C-A74C fiber as a robust scaffold for the reducer-free synthesis of Pd-Pt bimetallic materials, for achieving excellent electrocatalysis in HER under strongly alkaline condition. A previous report showed that Pd could be deposited onto wild-type TMV particles with a Pd precursor by heating at 50 °C for 30 min.⁴² We tested the controlled in-situ synthesis of Pd and Pt onto T103C-TMV-E50C-A74C fibers by simply heating (Figure S14). The reduction of Pt was much more difficult than Pd, which requires longer incubation time; but it is not a problem for T103C-TMV-E50C-A74C fibers that can stand heating at 50°C overnight (Figure S14C). We further synthesized cooperative, bimetallic electrocatalysts – Pd-Pt/TMV, with tunable ratios (Figure S15 and table S2), to achieve improved HER activity. The HER performance was investigated using a traditional three-electrode system in 1 mol/L KOH. The polarization curves in Figure S16 illustrate that the Pd-Pt(1:3)/TMV has best performance for alkaline hydrogen evolution.

Figures 5A,B show the morphology of Pd-Pt(1:3)/TMV. The uniform Pd-Pt coating on T103C-TMV-E50C-A74C fibers have a mean ~25-nm diameter and lengths of several micrometers. Given the 18-nm TMV diameter, the thickness of the Pt-Pd coating is around 3.5 nm. The crystalline nature of product was confirmed by high-resolution TEM (HRTEM) (Figure 5C). An interplanar spacing of 0.22 nm was observed, corresponding to the (111) plane of face-centered cubic Pd and Pt. The spatial distributions of Pd and Pt species were identified by HAADF-STEM and corresponding EDS elemental mapping, demonstrating that the Pd and Pt elements are homogeneously distributed on T103C-TMV-E50C-A74C fiber (Figure 5D). The

XRD in Figure 5E exhibits three diffraction peaks at 2θ values of 39.90, 46.39, and 67.62 degrees corresponding to the reflections from the (111), (200) and (220) planes. The angle shift of the peaks between those for Pd and Pt references indicates the alloy formation between metallic phases (Figure S17).⁵⁵ The ICP-MS measurement confirms the elemental compositions of Pd and Pt as 68.2% and 31.8%, respectively, in Pd-Pt(1:3)/TMV (Table S2). Figure 5F shows the HER electrocatalytic activity of Pd-Pt(1:3)/TMV in 1 mol/L KOH, and the structural integrity was verified under this condition (Figure S18). For comparison, Pd/TMV, Pt/TMV, and commercial 20 wt.% Pt/C were also investigated using the same deposition amount. Pd-Pt(1:3)/TMV exhibits much better HER activity than Pd/TMV and Pt/TMV. The prominent performance of Pd-Pt(1:3)/TMV in alkaline media is likely owing to the synergistic effect between these two components. It even reveals higher activity than commercial 20 wt.% Pt/C, showing a significant low overpotential of ~218 mV at a current density of 40 mA cm⁻², which is lower than that of the commercial 20% Pt/C (~309 mV) at the same current density. The mass density illustrates that the Pd-Pt(1:3)/TMV reaches a high current density of 430 mA mg⁻¹_{Pt-Pt} at an overpotential of 100 mV, which is 2.2 times that of commercial Pt/C (195 mA mg⁻¹_{Pt}) at the same overpotential (Figure S19).

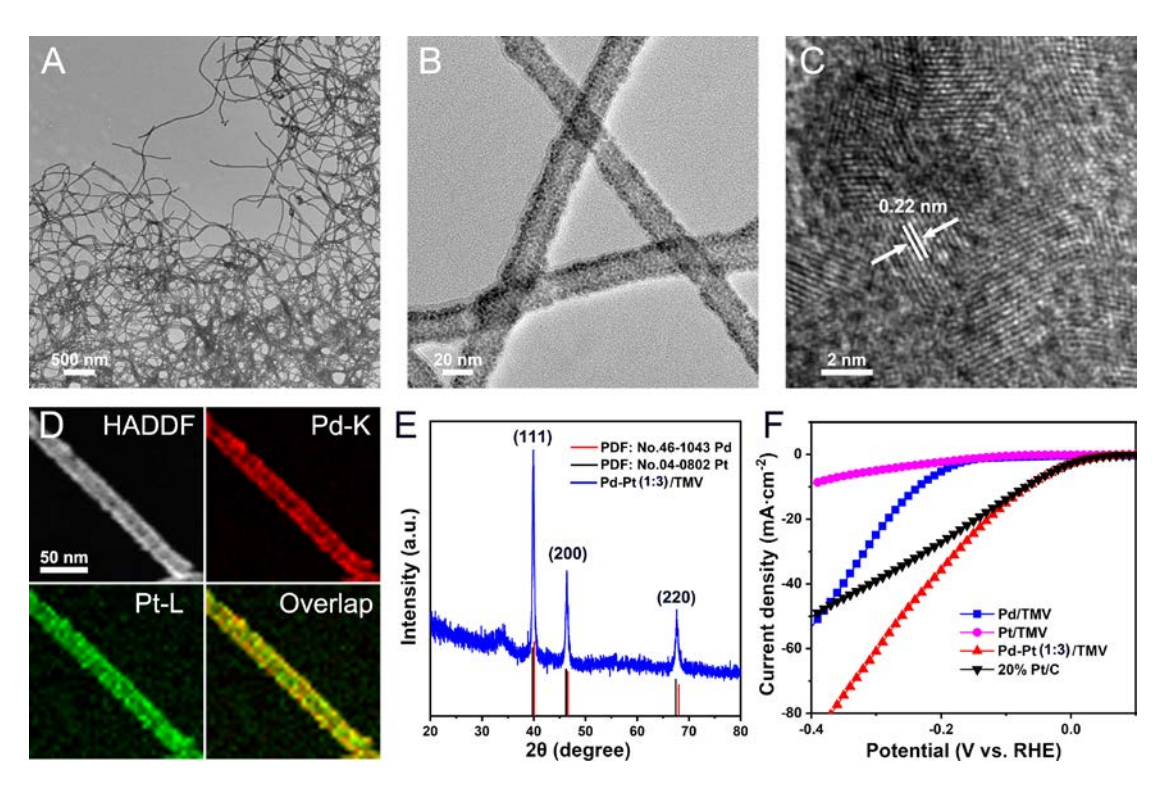


Figure 5. (A, B) TEM images of Pd-Pt(1:3)/TMV at different magnifications. (C) HRTEM image of Pd-Pt(1:3)/TMV. (D) The HAADF STEM image and corresponding EDS elemental mappings

of Pd-Pt(1:3)/TMV. (E) XRD pattern of Pd-Pt(1:3)/TMV in comparison with Pd and Pt reference. (F) HER polarization curves of Pd/TMV, Pt/TMV, Pd-Pt(1:3)/TMV, and commercial 20% Pt/C.

Conclusion

We have demonstrated the rational design of interfacially bridging covalent network to produce hyperstable and ultralong TMV VLPs which enable the application in fabricating electrocatalysts with exceptional performance for harshly alkaline hydrogen evolution. We conjugated every two adjacent T103C subunits into dimer in the lateral direction. Based on T103C-TMV, we engineered A74C Cys and investigated the evolution of Cys candidate ranging from E50C to P54C, to build disulfide bonds crossing longitudinal interfaces. T103C-TMV-E50C-A74C exhibits dramatically enhanced assembly capability and physical stability. Compared to previously reported TMV VLPs with a few hundred nanometers length, T103C-TMV-E50C-A74C fiber with lengths up to a dozen of micrometers displays remarkable alkali resistance under pH 13 condition. As the most robust TMV VLP to date, we applied it to in-situ synthesis of electrocatalyst for alkaline hydrogen evolution. The reducing agent-free synthesis of Pd, Pt, and Pd-Pt bimetallic crystals resulted in uniform coating layers along the protein fibers. The optimized Pd-Pt(1:3)/TMV showed outstanding HER performance in alkaline media. Apparently, more applications can be expected by using this developed TMV VLP template with hyperstability and ultralong length. This study provides a successful example of how to engineer covalent network within existing bioscaffold for achieving unprecedented structural properties and it can be a facile, efficient way to extend its functionality.

ASSOCIATED CONTENT

Supporting Information. Experimental details, additional TEM characterizations and analysis. This material is available in the online version of this article at http://XXX (automatically inserted by the publisher).

AUTHOR INFORMATION

Corresponding Author

E-mail: qbwang2008@sinano.ac.cn; yonggang.ke@emory.edu; huilejin@wzu.edu.cn

These authors contributed equally to this work.

ACKNOWLEDGMENT

This work was financially supported by the National Natural Science Foundation of China (Grant Nos. 21673280, 21977112, 21703282). Y.K. acknowledges the support of NSF grants DMR-1654485 and ECCS-1807568, and Semiconductor Research Corporation (SRC) grant 2018-SB-2836-B.

REFERENCES

- [1] C. E. Flynn, S.-W. Lee, B. R. Peelle, A. M. Belcher, *Acta Mater.* **2003**, *51*, 5867-5880.
- [2] T. Douglas, M. Young, Science **2006**, *312*, 873.
- [3] L. A. Lee, Z. Niu, Q. Wang, Nano Res. 2009, 2, 349-364.
- [4] S.-Y. Lee, J.-S. Lim, M. T. Harris, *Biotechnol. Bioeng.* **2012**, *109*, 16-30.
- [5] F. Li, Q. Wang, Small **2014**, 10, 230-245.
- [6] J. N. Culver, A. D. Brown, F. Zang, M. Gnerlich, K. Gerasopoulos, R. Ghodssi, *Virology* 2015, 479, 200-212.
- [7] A. M. Wen, N. F. Steinmetz, Chem. Soc. Rev. 2016, 45, 4074-4126.
- [8] C. M. Soto, B. R. Ratna, Curr. Opin. Biotechnol. 2010, 21, 426-438.
- [9] M. G. Mateu, *Protein Eng. Des. Sel.* **2010**, *24*, 53-63.
- [10] Z. Niu, M. Bruckman, V. S. Kotakadi, J. He, T. Emrick, T. P. Russell, L. Yang, Q. Wang, ChemComm 2006, 3019-3021.
- [11] A. A. Vernekar, G. Berger, A. E. Czapar, F. A. Veliz, D. I. Wang, N. F. Steinmetz, S. J. Lippard, J. Am. Chem. Soc. 2018, 140, 4279-4287.
- [12] R. A. Miller, N. Stephanopoulos, J. M. McFarland, A. S. Rosko, P. L. Geissler, M. B. Francis, J. Am. Chem. Soc. 2010, 132, 6068-6074.
- [13] C. Hou, Q. Luo, J. Liu, L. Miao, C. Zhang, Y. Gao, X. Zhang, J. Xu, Z. Dong, J. Liu, ACS Nano 2012, 6, 8692-8701.
- [14] M. L. Smith, W. P. Fitzmaurice, T. H. Turpen, K. E. Palmer, Curr. Top. Microbiol. Immunol. 2009, 332, 13-31.

- [15] aE. Dujardin, C. Peet, G. Stubbs, J. N. Culver, S. Mann, *Nano Lett.* **2003**, *3*, 413-417;
- [16] W. Shenton, T. Douglas, M. Young, G. Stubbs, S. Mann, Adv. Mater. 1999, 11, 253-256.
- [17] H. Wang, A. Planchart, G. Stubbs, *Biophys. J.* **1998**, *74*, 633-638.
- [18] B. Lu, G. Stubbs, J. N. Culver, Virology 1996, 225, 11-20.
- [19] J. Alonso, M. Górzny, A. Bittner, *Trends Biotechnol.* **2013**, *31*, 530-538.
- [20] K. Zhou, S. Eiben, Q. Wang, ACS Appl. Mater. Interfaces 2016, 8, 13192-13196.
- [21] A. D. Brown, L. Naves, X. Wang, R. Ghodssi, J. N. Culver, *Biomacromolecules* 2013, 14, 3123-3129.
- [22] Y. Tian, M. Zhou, H. Shi, S. Gao, G. Xie, M. Zhu, M. Wu, J. Chen, Z. Niu, *Nano Lett.* 2018, 18, 5453-5460.
- [23] H. Hu, Y. Zhang, S. Shukla, Y. Gu, X. Yu, N. F. Steinmetz, ACS Nano 2017, 11, 9249-9258.
- [24] S. Shukla, F. J. Eber, A. S. Nagarajan, N. A. DiFranco, N. Schmidt, A. M. Wen, S. Eiben, R. M. Twyman, C. Wege, N. F. Steinmetz, *Adv. Healthc. Mater.* **2015**, *4*, 874-882.
- [25] Y. Wu, S. Feng, X. Zan, Y. Lin, Q. Wang, Biomacromolecules 2015, 16, 3466-3472.
- [26] J. A. Luckanagul, K. Metavarayuth, S. Feng, P. Maneesaay, A. Y. Clark, X. Yang, A. J. García, Q. Wang, ACS Biomater. Sci. Eng. 2016, 2, 606-615.
- [27] P. Atanasova, D. Rothenstein, J. J. Schneider, R. C. Hoffmann, S. Dilfer, S. Eiben, C. Wege, H. Jeske, J. Bill, *Adv. Mater.* **2011**, *23*, 4918-4922.
- [28] R. J. Tseng, C. Tsai, L. Ma, J. Ouyang, C. S. Ozkan, Y. Yang, *Nat. Nanotechnol.* **2006**, *1*, 72-77.
- [29] M. Ł. Górzny, A. S. Walton, S. D. Evans, Adv. Funct. Mater. 2010, 20, 1295-1300.
- [30] C. Yang, C.-H. Choi, C.-S. Lee, H. Yi, ACS Nano 2013, 7, 5032-5044.
- [31] K. Gerasopoulos, E. Pomerantseva, M. McCarthy, A. Brown, C. Wang, J. Culver, R. Ghodssi, *ACS Nano* **2012**, *6*, 6422-6432.
- [32] X. Chen, K. Gerasopoulos, J. Guo, A. Brown, C. Wang, R. Ghodssi, J. N. Culver, ACS Nano 2010, 4, 5366-5372.
- [33] V. Liljeström, A. Ora, J. Hassinen, H. T. Rekola, Nonappa, M. Heilala, V. Hynninen, J. J. Joensuu, R. H. A. Ras, P. Törmä, O. Ikkala, M. A. Kostiainen, *Nat. Commun.* **2017**, *8*, 671.
- [34] Z. Niu, J. Liu, L. A. Lee, M. A. Bruckman, D. Zhao, G. Koley, Q. Wang, *Nano Lett.* 2007, 7, 3729-3733.
- [35] Y. Lin, E. Balizan, L. A. Lee, Z. Niu, Q. Wang, Angew. Chem. Int. Ed. 2010, 49, 868-872.
- [36] M. Kobayashi, M. Seki, H. Tabata, Y. Watanabe, I. Yamashita, Nano Lett. 2010, 10, 773-776.
- [37] Z. Wu, A. Mueller, S. Degenhard, S. E. Ruff, F. Geiger, A. M. Bittner, C. Wege, C. E. Krill Iii, ACS Nano 2010, 4, 4531-4538.
- [38] S. Li, M. Dharmarwardana, R. P. Welch, Y. Ren, C. M. Thompson, R. A. Smaldone, J. J. Gassensmith, *Angew. Chem. Int. Ed.* **2016**, *55*, 10691-10696.
- [39] Y. Tian, X. Yan, M. L. Saha, Z. Niu, P. J. Stang, J. Am. Chem. Soc. 2016, 138, 12033-12036.
- [40] F. J. Eber, S. Eiben, H. Jeske, C. Wege, Angew. Chem. Int. Ed. 2013, 52, 7203-7207.
- [41] T. Li, X. Zan, R. E. Winans, Q. Wang, B. Lee, Angew. Chem. Int. Ed. 2013, 52, 6638-6642.
- [42] J.-S. Lim, S.-M. Kim, S.-Y. Lee, E. A. Stach, J. N. Culver, M. T. Harris, *Nano Lett.* **2010**, *10*, 3863-3867.
- [43] K. Zhou, F. Li, G. Dai, C. Meng, Q. Wang, Biomacromolecules 2013, 14, 2593-2600.
- [44] A. V. Kachur, C. J. Koch, J. E. Biaglow, Free Radic. Res. 1999, 31, 23-34.
- [45] R. Sanchez, M. Riddle, J. Woo, J. Momand, *Protein Sci.* **2008**, *17*, 473-481.

- [46] W. L. DeLano, CCP4 Newslett. Protein Crystallogr. 2002, 40, 82-92.
- [47] M.-a. Sun, Y. Wang, Q. Zhang, Y. Xia, W. Ge, D. Guo, BMC Genom. 2017, 18, 279.
- [48] M. Knez, M. Sumser, A. M. Bittner, C. Wege, H. Jeske, T. P. Martin, K. Kern, Adv. Funct. Mater. 2004, 14, 116-124.
- [49] V. N. Orlov, A. M. Arutyunyan, S. V. Kust, E. A. Litmanovich, V. A. Drachev, E. N. Dobrov, *Biochemistry* **2001**, *66*, 154-162.
- [50] J. M. Toedt, E. H. Braswell, T. M. Schuster, D. A. Yphantis, Z. F. Taraporewala, J. N. Culver, *Protein Sci.* **1999**, *8*, 261-270.
- [51] D. Schubert, B. Krafczyk, *Biochim. Biophys. Acta.* **1969**, *188*, 155-157.
- [52] A. Arutyunyan, E. Rafikova, V. Drachev, E. Dobrov, *Biochemistry* **2001**, *66*, 1378-1380.
- [53] Y.-W. Lee, A.-R. Ko, S.-B. Han, H.-S. Kim, K.-W. Park, *Phys. Chem. Chem. Phys.* **2011**, *13*, 5569-5572.

Table of contents

